SUPPORTING INFORMATION

TITLE: Environmental and genetic factors support the dissociation between alpha-synuclein aggregation and toxicity
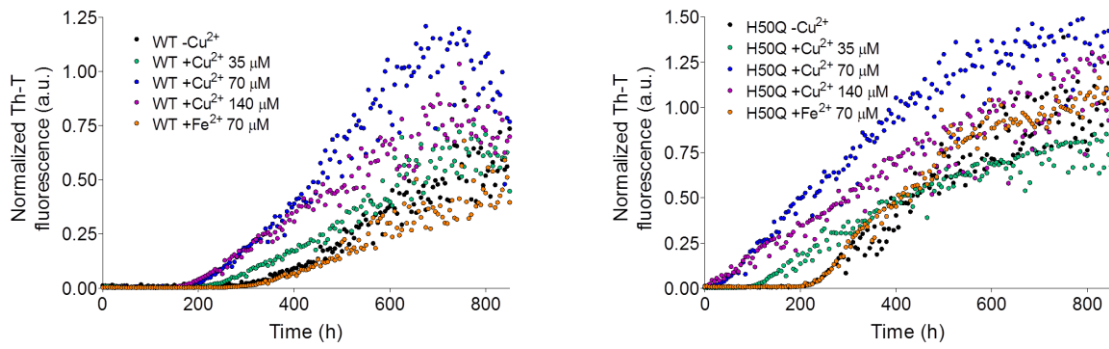
SI Fig. S1

H50Q accumulation occurs specifically as an effect of treatment with Cu^{2+}. To study the specificity of the interaction between H50Q mutation and Cu^{2+}, Iron II, Iron III and Zinc were added to the media in the presence of H4 cells transfected with H50Q, where no intracellular accumulation was observed. (Scale bar, 5 μm.)
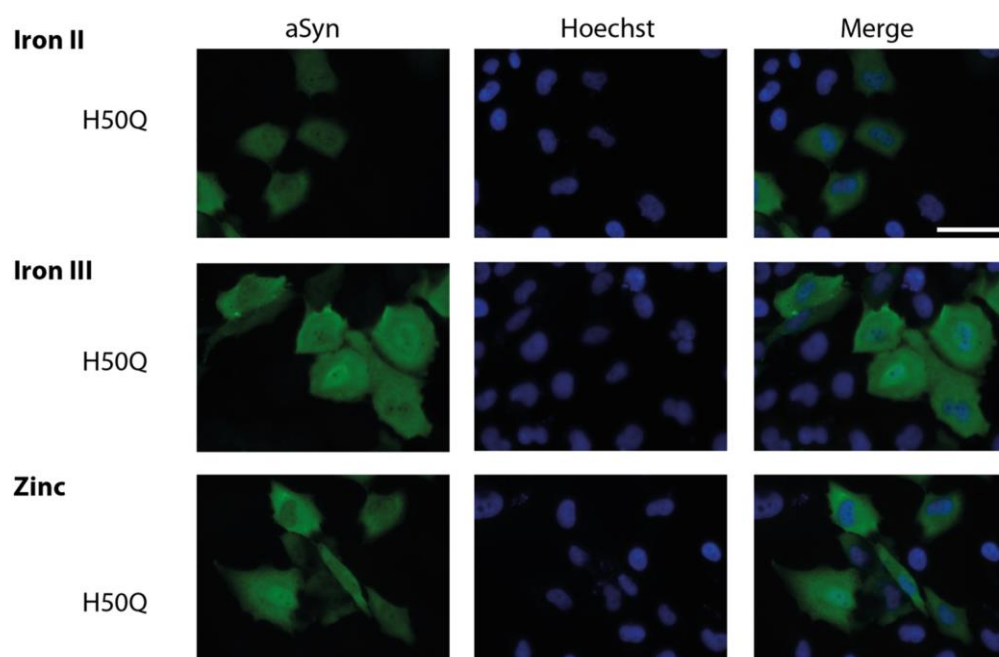
SI Fig. S2

aSyn aggregation dependency on different Cu^{2+} concentrations and Fe^{2+}. Aggregation kinetics of WT (*Left*) and H50Q (*Right*) aSyn were followed by Th-T fluorescence in a 96 well plate assay using the indicated metal concentrations.

SI Fig. S3

Secondary structure determination of aSyn aggregates. A. CD spectra of each aggregate at initial and end time point of the aggregation kinetics (discontinuous and continuous lines, respectively). **B.** ATR-FTIR spectra (continuous line) and their corresponding deconvolution spectra (discontinuous lines) of each aggregate at the end time point of the aggregation kinetics. **C.** ANS binding assay performed with the final aggregates (*Left*) and with the soluble samples at their monomeric stage (*Right*). Since soluble aSyn does not bind ANS, transthyretin spectra was included as a positive control.
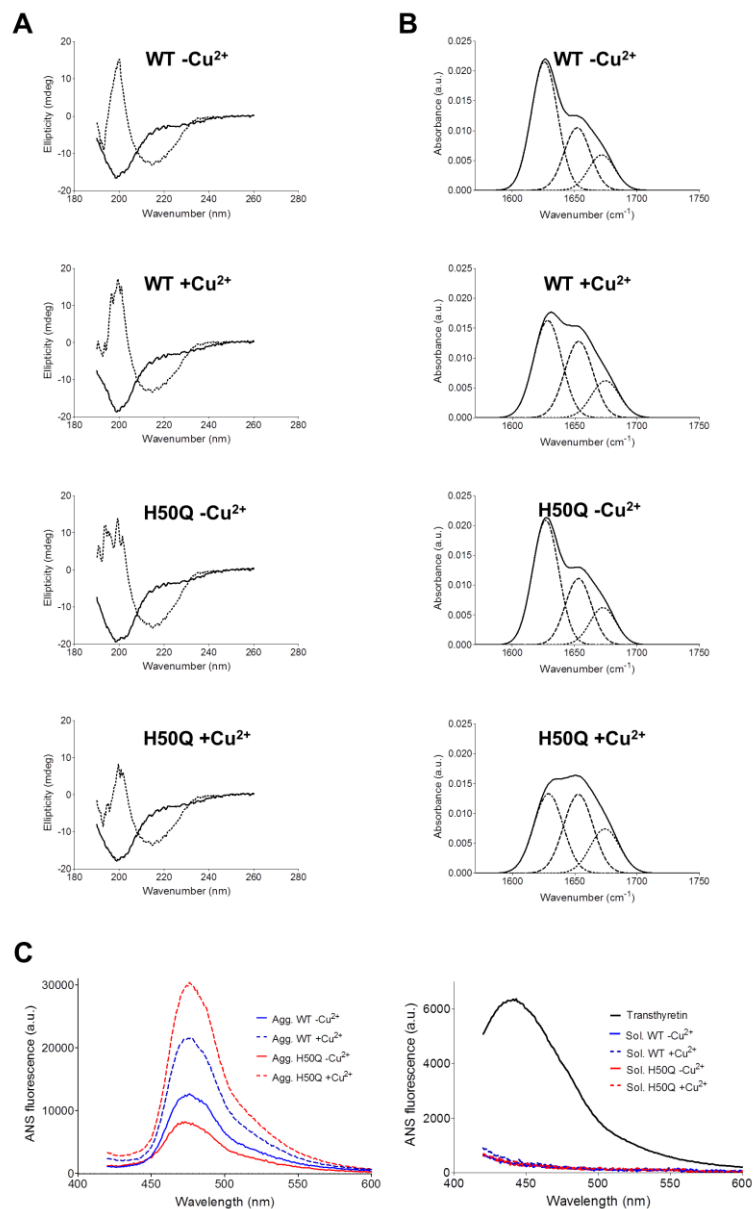
SI Fig. S4

Pattern of PK-resistant fragments after partial proteolysis. Partial PK digestion of the aggregates visualized by WB using 2 different antibodies, Syn-1 and C-20, with epitopes located in the central and C-terminal region, respectively. Each lane represents different digestion times: 0, 1, 2.5, 5 and 10 min. MW, molecular weight/molecular mass.
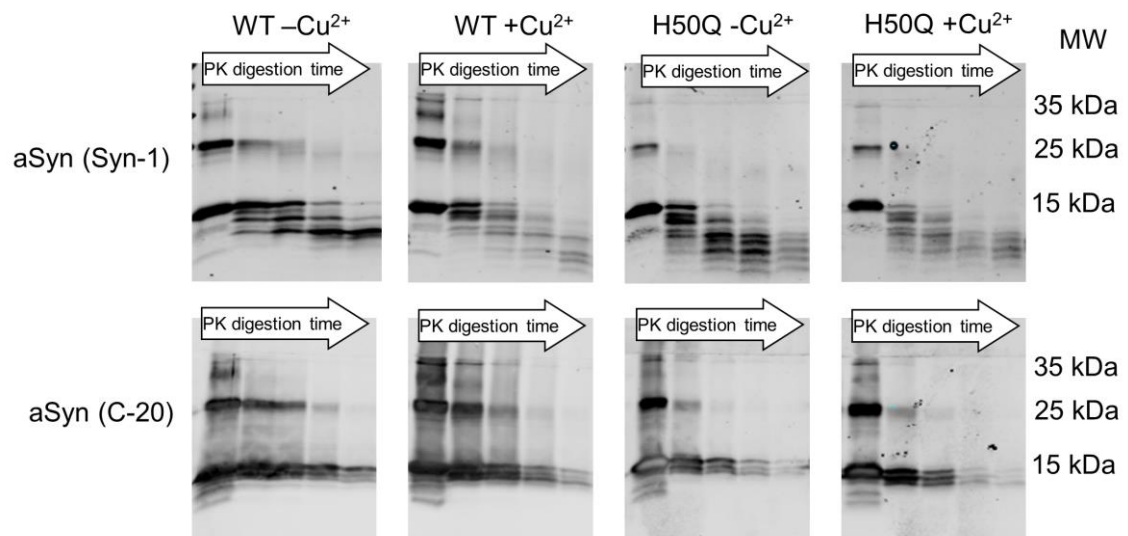
SI Molecular simulations (MS)

Section MS.1. Models C, D, E. In model **C**, the three additional ligands to the imidazole N of H50 are G51 and V52 deprotonated amides, along with V52 carbonyl (1). Here, the Cu^{2+} is coordinated in a 7-membered-ring (see Chart Insert in Fig. MS.1). The latter is a rather unlikely coordination (2). QM/MM simulations lead to a pyramidal coordination geometry: the square basis are ligands from G51 and V52, while a water molecule is located at the top of the pyramid (see Fig. MS.1-1). This coordination is not consistent with EPR data (3, 4). Model **C** is therefore discarded. Models **D** and **E** are proposed by us here for the first time. The three additional ligands to H50 side chain are V49 deprotonated amide group, V48 backbone carbonyl, and either a water molecule (model **D**) or H50 deprotonated amide group (model **E**), see Chart Insert in Fig. MS.1. We could identify only one conformation fitting each pose from N-terminally acetylated aSyn (Ac_aSyn) conformational ensemble generated in (5). However, even in these conformations, the copper coordination polyhedron turned out to be very much distorted. In particular, the C=O(V48)····Cu angle was lower than 70°in both the modes. Attempting at relaxing the structures by QM/MM dynamics lead to the detachment of the copper ion from the protein (Fig. MS.1-2,3 and Fig. MS.1-4,5 for model **D** and **E**, respectively) already in less of 1 ps. Hence, model **D** and **E** were also discarded.

Section MS.2. Details on Criterion (iii) for selections of Ac_aSyn conformers. Let us define the function $f(d_n)$ ($Å^2$), where n is the number of distances (d) between copper's ligands on which the selection criteria are applied. For models **A**, **B** and **D** (see insert of Fig. MS.1): $f(d_1,d_2,d_3)$ ($Å^2$) $= (d_1 - 2.9)^2 + (d_2 - 4.4)^2 + (d_3 - 2.9)^2$ (1), where: d_1 is the distance between Imidazole N from H50 (N_{im}) and L1, d_2 is the distance between N_{im} and L2, d_3 is the distance between L1 and L2. L1, L2 denote N(V49) and O(V48) in **D;** N(H50) and O(V48) in **A;** and N(H50) and N(V49) in **B**. A water molecule completes the copper coordination. Because water molecules change during the QM/MM simulations, distances involving the water molecule are not included in the function f. For models **C** and **E** (see insert of Fig. MS.1): $f(d_1,d_2,d_3,d_4)$ ($Å^2$) $= (d_1 - 2.9)^2 + (d_2 - 2.9)^2 + (d_3 - 2.9)^2 + (d_4 - 2.9)^2$ (2), where: d_1 is the distance between N_{im} and L1, d_2 is the distance between N_{im} and L3, d_3 is the distance between L1 and L2, d_4 is the distance between L2 and L3, L1, L2 and L3 denote N(H51), N(V52) and O(V52) in **C** and N(H50), N(V49), O(V48) in **E**. The conformations featuring the smallest values of the function f are here considered.

Section MS.3. Force-field based energy minimization and MD simulations. The Cu^{2+}-aSyn complexes in explicit solvent representing poses **a-e** underwent 3200 conjugate gradients step-based energy minimization. Then, the systems were heated up from 0 to 300 K in a stepwise linear manner for 300 ps of MD. The target temperatures was achieved by using the Berendsen thermostat and barostats (6). 4 ns MD were then performed in the NPT ensemble at 300 K with a Nosé-Hoover thermostat (7-9) and a Parrinello-Rahman barostat (10). Periodic boundary conditions were applied. A distance of 10 Å or more separated the biomolecular complex from its images. The particle mesh Ewald (PME) method (11) was used to calculate long-range electrostatic interactions. Van der Waals and the real part of the Coulomb interactions were truncated at 12 Å. The time-step was set to 1 fs. Bond lengths were not fixed.

Section MS.4. Heating protocol for QM/MM molecular dynamics. First we heated our systems up to 25 K with a Berendsen thermostat (6) during 0.121 ps, increasing the temperature linearly at a rate of 0.827 K/fs, until we reached 25 K. Then we equilibrated the system at 25 K by means of two Nosé-Hoover thermostats (7, 8) (one applied to the protein, Cu and water bound to Cu, and the other one applied to the rest of the system, in order to avoid the hot solvent-cold solute problem) during 0.242 ps. Once the system was equilibrated at 25 K, we increased again the temperature with a Berendsen thermostat during 0.121 ps until we reach 50 K at a rate of 2.06 K/fs. Afterwards, we equilibrated the system at 50 K with two Nosé-Hoover thermostats (7-9), as we did at 25 K. We increased the temperature from 50 to 75 K and from 75 to 100 K as we did from from 25 to 50. Then we heated the system up to 150 K at a rate of 1.24 K/fs using the Berendsen thermostat during 0.242 ps. Again, we equilibrated the system at 150 K with two Nosé-Hoover thermostats (7, 12). The same protocol for heating the system from 100 to 150 K was used in order to increase the temperature from 150 to 200 K, from 200 to 250 K and from 250 to 300 K.

Section MS.5A. Molecular Simulations. The second binding site of aSyn is basically the same as the first binding site of Ac_aSyn. Here we model the latter which has relevance also for the second binding site of copper studied here. We selected nine conformations of Ac_aSyn in aqueous solution from the Ac_aSyn ensemble in explicit solvent reported in ref. (5). The selection was based on the following criteria: **(i)** Cu^{2+} could dock in either pose A, B, or C, or D, or E (Chart 1 in insert of Fig. MS.1) by following the geometrical criteria described in Section MS.2 and Fig. MS.1; **(ii)** The geometry of the Cu^{2+}) coordination polyhedron was consistent with experiment, namely it was either square planar or distorted tetrahedron (3). **(iii)** The four metal ion–donors atom distances are close to 2.2 Å (see Fig. MS.1) **(iv)** The calculated NMR chemical shifts of the C_α, C_β, and N atoms for the Ac_aSyn conformations that fulfil criteria (i) to (iii) agree best with the corresponding experimental data (13). 1, 1, 1, 3, 3 conformations could be selected for A, B, C, D, E, respectively. A Cu^{2+} ion was docked on each of them. The 9 adducts underwent molecular simulations always in explicit solvent and counter ions inserted a orthorhombic simulation box (Table. MS.3) following the same protocol of ref. (5) (Section MS.3). A first round of Car-Parrinello quantum-mechanics/classical mechanics (QM/MM) simulations (14) was performed on these models in explicit solvent. The QM part consisted of the Cu^{2+} ion, residues H50 and G51 along with V48 and V49 backbone units (except for model **C**, where residues H50, G51, A53 and V52 backbone units were considered as QM). It was treated at the density functional theory (DFT) level with the BLYP exchange-correlation functional (15, 16). We used a plane-wave basis set with an energy cutoff of 80 Ry, a fictitious mass of 400 a. u. for the electrons and a time step of 0.097 fs. Isolated system conditions were achieved by using the Martina-Tuckerman scheme (17). The MM part included the protein frame, the solvent and counter ions in an octahedral box (see dimensions for each system in Table MS.2). It was described by the ffAMBER99SB force field (18) with the ILDN modification (19) for the protein and the ions, and the TIP3P water model (20). The C_α-C dangling bonds of the residues binding to the metal ion were saturated by dummy, monovalent C atoms with an apt pseudopotential (21). Periodic boundary conditions were applied. A distance of 10 Å or more separated the biomolecular complexes from their images. After heating the systems from 0 to 300 K in 0.73 ps, the temperature was kept at 300 K using a Nosé-Hoover thermostat (7, 12) for 3.87 ps (Section MS.4). After the annealing, model **C**

assumed a coordination geometry not compatible with experiments (Section MS.1 and Fig. MS.1), therefore it was not considered for further calculations. During the first round of QM/MM simulations, models **D** and **E** turned out to be unstable (Section MS.1 and Fig. MS.1). Therefore, they were also not considered for further calculations. Complexes **A** and **B** underwent classical molecular dynamics simulations. To this aim, we constructed a force field for the copper coordination polyhedron using a force-matching procedure from our previous QM/MM simulations (22). After energy- minimizing and warming up the system from 0 to 300 K, 4 ns of classical MD in explicit solvent were carried out. Six selected MD conformers in explicit solvent that best satisfied criteria (i)-(ii) underwent Car-Parrinello QM/MM annealing from 300 K to 0 K (decreasing 3.3 % of the temperature every fs). Square planar geometry was always kept, therefore, we considered that it was more stable that the distorted tetrahedral geometry. They were then heated up to 300 K in 3.5 ps. The same setup for the QM/MM as first round of QM/MM was used. Finally, 30 ps QM/MM simulations were run for each system. The CPMD program along with the GROMOS96 code (14, 23) and the GROMACS codes (24), were used, respectively from the QM/MM and MD simulations.

Section MS.5B. Accuracy of the predictions. As in any modeling study, there are issues that limit the accuracy of the calculations. These may be even more acute for an intrinsically disordered protein such as aSyn, for which long time scales may be required to explore the very large conformational space. Possible large conformational changes of Ac_aSyn due to the presence of the metal ion cannot be obviously be predicted by our QM/MM calculations, which are necessarily limited to the subns timescale. Procedures such as the force matching on top of the QM/MM calculations, used by several groups including ours (25, 26), may help alleviate this issue. In spite of this caveat, we stress here that our simulations do provide the first models of Ac_aSyn in explicit solvent in complex with Cu^{2+}, consistent with experimental data. An additional limitation is given by the predictive power of biomolecular force fields. For consistency with previous calculations of Ac_aSyn (5, 27, 28), fully consistent with a large wealth of experimental data, we use the ffAMBER99SB force field (18) with the ILDN modification (19). This has been constructed for structural proteins and its domain of applicability may be limited for intrinsically disordered proteins. Use of recent modifications, such as that of Piana et al. (29), may lead to a further improved predictive power.

Table MS.1: Selected geometrical parameters for the three starting structures of our QM/MM calculations of models **A** and **B**. Distances are reported in Å and angles in degrees.

A				B			
Distances							
Poses	*1*	*2*	*3*	*Poses*	*1*	*2*	*3*
N_{im}-Cu	1.97	2.00	1.97	N_{im}-Cu	2.08	1.99	2.14
N(H50)-Cu	1.98	2.05	1.91	N(H50)-Cu	2.16	2.17	2.14
O(V48)-Cu	1.71	1.92	1.89	N(V49)-Cu	2.24	2.13	2.09
O_w-Cu	1.89	1.89	2.00	O_w-Cu	2.16	2.03	2.17
Angles							
N_{im}-Cu-O_w	95°	92°	91°	N_{im}-Cu-O_w	85°	83°	83°
O_w-Cu-O(V48)	72°	71°	71°	O_w-Cu-N(V49)	103°	100°	107°
O(V48)-Cu-N(H50)	97°	99°	95°	N(V49)-Cu-N(H50)	83°	83°	91°
N(H50)-Cu-N_{am}	93°	93°	96°	N(H50)-Cu-N_{im}	90°	95°	84°

Table MS.2: Selected structural parameters for models **A** and **B**. Averages distances and angles over the 30 ps of QM/MM simulations are reported in Å and in degrees, respectively.

A				B			
Distances							
Poses	*1*	*2*	*3*		*1*	*2*	*3*
N_{im}-Cu	2.05±0.07	2.04±0.06	2.06±0.07	N_{im}-Cu	2.08±0.07	2.04±0.06	2.08±0.07
N(H50)-Cu	2.10±0.09	2.01±0.05	2.00±0.06	N(H50)-Cu	1.99±0.05	2.04±0.06	2.02±0.06
O(V48)-Cu	2.3±0.4	2.2±0.1	2.4±0.2	N(V49)-Cu	2.3±0.1	2.06±0.06	2.11±0.08
O_w-Cu	2.10±0.09	2.07±0.07	2.06±0.07	O_w-Cu	2.09±0.08	2.14±0.09	2.10±0.09
Angles							
N_{im}-Cu-O_w	91±6	94±4	99±6	N_{im}-Cu-O_w	91±5	89±4	93±5

O$_w$-Cu-O(V48)	75±7	84±5	78±6	O$_w$-Cu-N(V49)	100±4	96±4	97±4
O(V48)-Cu-N(H50)	99±5	92±4	91±4	N(V49)-Cu-N(H50)	78±3	83±3	83±3
N(H50)-Cu-N$_{am}$	96±4	90±3	91±4	N(H50)-Cu-N$_{im}$	91±3	90±3	90±3

Table MS.3: Details of the structures used on our QM/MM MD calculations. All systems are electrically neutral.

	Cell size (nm)	number of water molecules	number of Na$^+$ ions	Total number of atoms
Model **D**	99×145× 65	29997	9	92020
Model **E**	99×145× 65	29997	10	92021
Model **A** – pose 1	123×80× 120	38121	9	116392
Model **A** – pose 2	83×131× 73	25443	9	78358
Model **A** – pose 3	88×102× 86	32668	9	100033
Model **B** – pose 1	123×80× 120	38121	10	116393
Model **B** – pose 2	90×151× 110	47840	10	145550
Model **B** – pose 3	88×102× 86	32668	10	100034
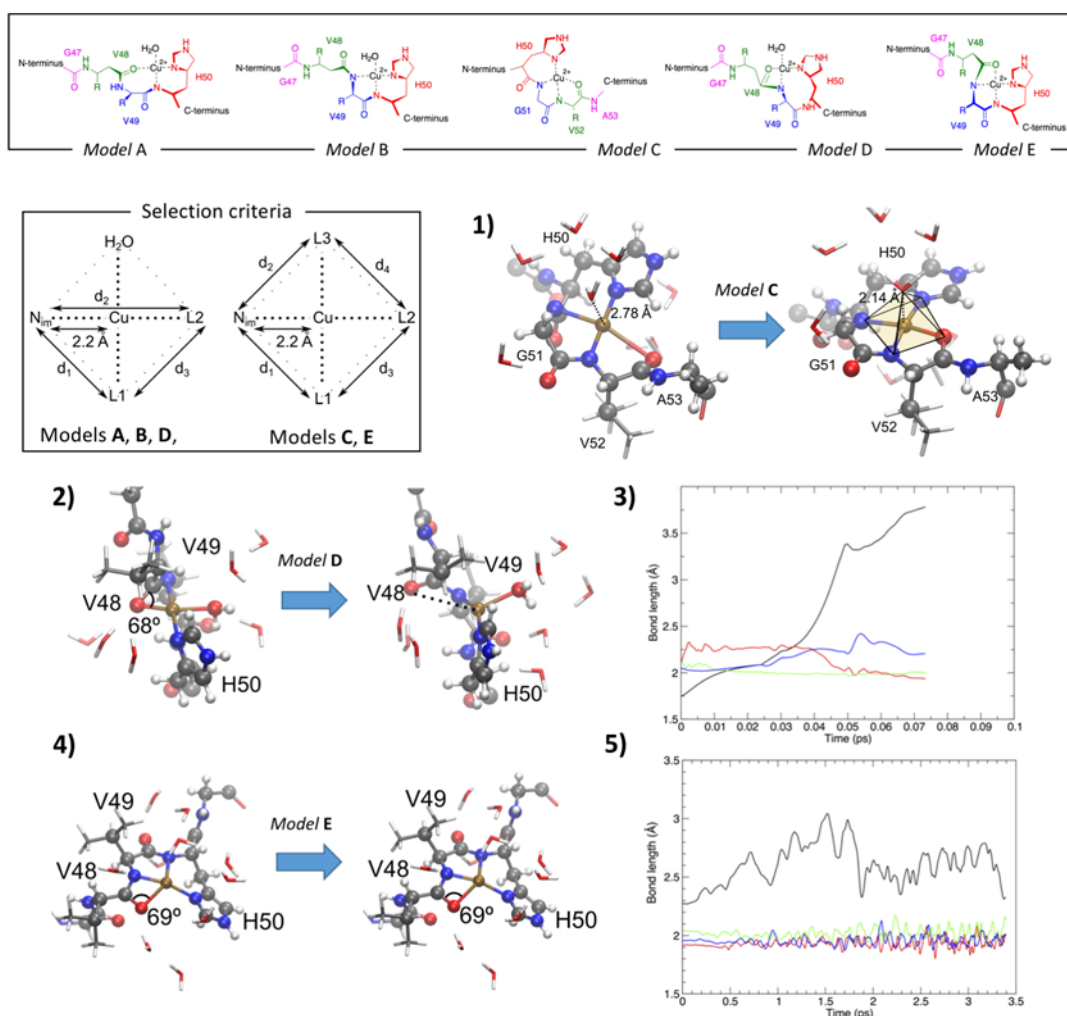
Figure MS.1: **Inserts**: On the Top a charter of the Cu^{2+}-Ac_aSyn models compatible with experiments, on the side, the selection criteria (Section MS.3) are offered. **1)** Model **C**: Initial Cu^{2+} ion pose and its geometry after the annealing; **2)** Model **D**: Cu^{2+} ion pose in the first round of QM/MM simulations at t=0 ps and t=2 ps; **3)** Cu^{2+}-O(V48), Cu^{2+}-N(49), Cu^{2+}-N(imidazole), Cu^{2+}-O(water) as a function of time are shown for model **D**. In less than 0.05 ps (i. e. during the annealing process), the V48 carbonyl-O-Cu is completely broken (d(Cu-O) = 3.0 Å). **4)** Model **E**: Cu^{2+} ion pose in the first round of QM/MM simulations at t=0 ps and t=2 ps; **5)** Cu^{2+}-O(V48), Cu^{2+}-N(V49), Cu^{2+}-N(H50), Cu^{2+}-N$_{Imidazole}$ bond distances plotted as a function of time for model **E**. After 1.5 ps, the V48 carbonyl-O–Cu bond is completely broken. Bond distances in plot 3) and 5) are colored in black, red, green, blue, respectively.
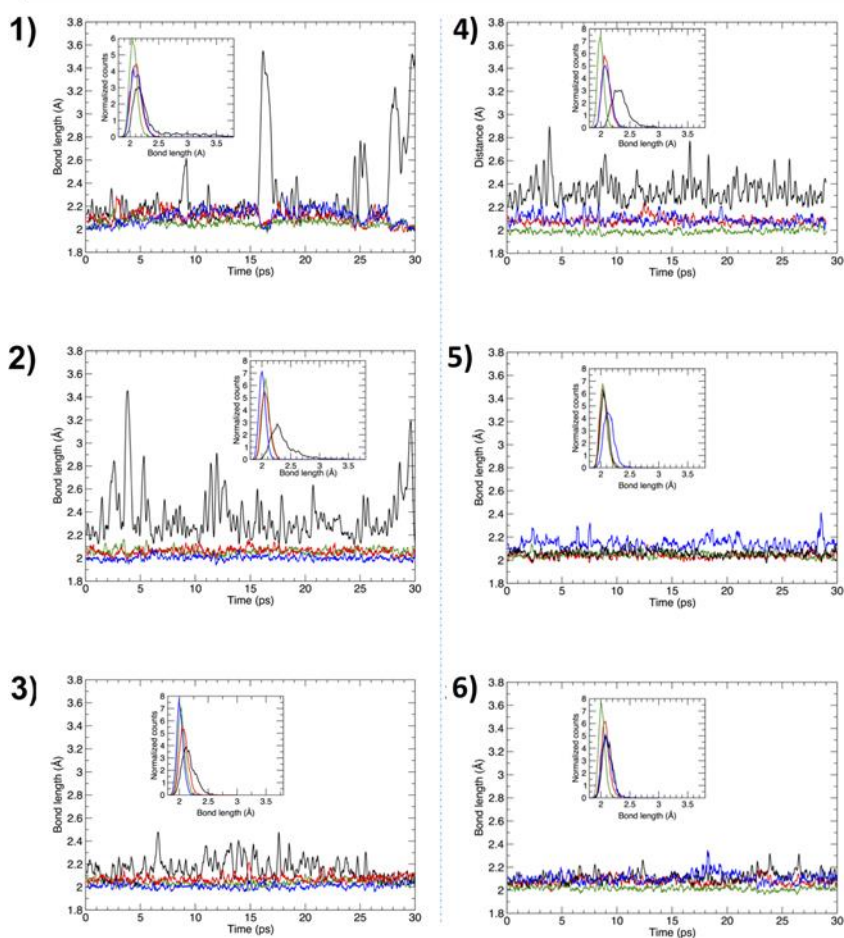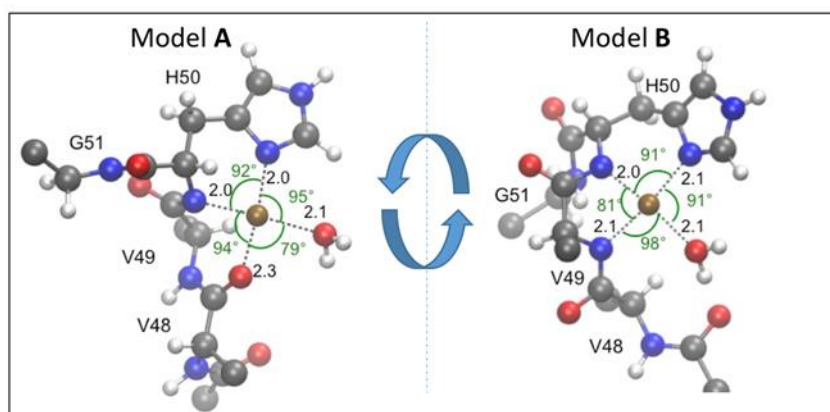
Figure MS.2: **Insert**: Geometries and average angles and distances of model **A** and **B**. **1)**-**2)**-**3)** Cu^{2+}-ligands bond lengths over time for the three poses of model **A**: Cu-O (carboxylic oxygen from V48), black lines; Cu-O (water), red lines; Cu-N (imidazole N), green lines; Cu-N (amide from H50), blue lines. Inset, histogram of the bond lengths for each of the ligands. **4)**-**5)**-**6):** Cu^{2+}-ligands bond lengths over time for the three poses of model **B**: Cu-N (amide from V49), black line; Cu-N (imidazole N), red line; Cu-N (amide from H50), green line; Cu-O (amide from water), blue line. Inset, histogram of the bond length for each of the ligands.

References of SI Molecular simulations (MS)

1.   Rose F, Hodak M, & Bernholc J (2011) Mechanism of copper(II)-induced misfolding of Parkinson's disease protein. *Scientific reports* 1:11.
2.   Sóvágó I, Kállay C, & Várnagy K (2012) Peptides as complexing agents: Factors influencing the structure and thermodynamic stability of peptide complexes. *Coordination Chemistry Reviews* 256(19-20):2225-2233.
3.   Rasia RM*, et al.* (2005) Structural characterization of copper(II) binding to alpha-synuclein: Insights into the bioinorganic chemistry of Parkinson's disease. *Proc Natl Acad Sci USA* 102(12):4294-4299.
4.   Kowalik-Jankowska T, Rajewska A, Jankowska E, & Grzonka Z (2006) Copper(II) binding by fragments of alpha-synuclein containing M1-D2- and -H50-residues; a combined potentiometric and spectroscopic study. *Dalton Trans* (42):5068-5076.
5.   Rossetti G*, et al.* (2016) Conformational ensemble of human alpha-synuclein physiological form predicted by molecular simulations. *Phys Chem Chem Phys* 18(8):5702-5706.
6.   Berendsen H, Postma J, Vangunsteren W, Di Nola A, & Haak J (1984) Molecular-Dynamics with Coupling to an External Bath. *J Chem Phys* 81(8):3684-3690.
7.   Nose S (1984) A molecular dynamics method for simulations in the canonical ensemble. *Molecular Physics* 52(2):255-268.
8.   Hoover WG (1985) Canonical dynamics - equilibrium phase-space distributions. *Phys. Rev. A* 31(3):1695-1697.
9.   Parrinello M & Rahman A (1981) Polymorphic Transitions in Single-Crystals - a new Molecular-Dynamics Method. *J Appl Phys* 52(12):7182-7190.
10.   Parrinello M & Rahman A (1981) Polymorphic transitions in single crystals: A new molecular dynamics method. *J Appl Phys* 52(12):7182-7190.
11.   Darden T, York D, & Pedersen L (1993) Particle mesh Ewald: An N· log (N) method for Ewald sums in large systems. *J Chem Phys* 98(12):10089-10092.
12.   Hoover W (1985) Canonical dynamics: Equilibrium phase-space distributions. *Phys. Rev. A* 31(3):1695-1697.
13.   Roche J, Ying J, Maltsev AS, & Bax A (2013) Impact of Hydrostatic Pressure on an Intrinsically Disordered Protein: A High-Pressure NMR Study of α-Synuclein. *ChemBioChem* 14(14):1754-1761.
14.   Laio A, VandeVondele J, & Rothlisberger U (2002) A Hamiltonian electrostatic coupling scheme for hybrid Car-Parrinello molecular dynamics simulations. *J. Chem. Phys.* 116(16):6941-6947.
15.   Becke AD (1988) Density-Functional Exchange-Energy Approximation with Correct Asymptotic-Behavior. *Phys Rev A* 38(6):3098-3100.
16.   Lee CT, Yang WT, & Parr RG (1988) Development of the Colle-Salvetti Correlation-Energy Formula into a Functional of the Electron-Density. *Phys Rev B* 37(2):785-789.
17.   Martyna G & Tuckerman M (1999) A reciprocal space based method for treating long range interactions in ab initio and force-field-based calculations in clusters. *J Chem Phys* 110(6):2810-2821.
18.   Hornak V*, et al.* (2006) Comparison of multiple Amber force fields and development of improved protein backbone parameters. *Proteins* 65(3):712-725.
19.   Lindorff-Larsen K*, et al.* (2010) Improved side-chain torsion potentials for the Amber ff99SB protein force field. *Proteins* 78(8):1950-1958.
20.   Jorgensen W, Chandrasekhar J, Madura J, Impey R, & Klein M (1983) Comparison of simple potential functions for simulating liquid water. *J Chem Phys* 79(2):926-935.

21.   von Lilienfeld OA, Tavernelli I, Rothlisberger U, & Sebastiani D (2005) Variational optimization of effective atom centered potentials for molecular properties. *Journal of Chemical Physics* 122(1):14113.

22.   Maurer P, Laio A, Hugosson HW, Colombo MC, & Rothlisberger U (2007) Automated parametrization of biomolecular force fields from quantum mechanics/molecular mechanics (QM/MM) simulations through force matching. *J Chem Theory Comput* 3(2):628-639.

23.   van Gunsteren WF*, et al.* (1996) Biomolecular Simulation: The GROMOS96 Manual and User Guide. Vdf Hochschulverlag AG an der ETH Zurich, Zurich.

24.   Hess B, Kutzner C, van der Spoel D, & Lindahl E (2008) GROMACS 4: Algorithms for Highly Efficient, Load-Balanced, and Scalable Molecular Simulation. *J. Chem. Theory Comput.* 4(3):435-447.

25.   Doemer M, Maurer P, Campomanes P, Tavernelli I, & Rothlisberger U (2013) Generalized QM/MM Force Matching Approach Applied to the 11-cis Protonated Schiff Base Chromophore of Rhodopsin. *J Chem Theory Comput* 10(1):412-422.

26.   Spiegel K*, et al.* (2008) Parameterization of azole-bridged dinuclear platinum anticancer drugs via a QM/MM force matching procedure. *Journal of Computational Chemistry* 29(1):38-49.

27.   Herrera FE*, et al.* (2008) Inhibition of alpha-synuclein fibrillization by dopamine is mediated by interactions with five C-terminal residues and with E83 in the NAC region. *PLoS ONE* 3(10):e3394.

28.   Dibenedetto D, Rossetti G, Caliandro R, & Carloni P (2013) A molecular dynamics simulation-based interpretation of nuclear magnetic resonance multidimensional heteronuclear spectra of alpha-synuclein.dopamine adducts. *Biochemistry* 52(38):6672-6683.

29.   Piana S, Donchev AG, Robustelli P, & Shaw DE (2015) Water Dispersion Interactions Strongly Influence Simulated Structural Properties of Disordered Protein States. *J. Phys. Chem. B* 119(16):5113-5123.
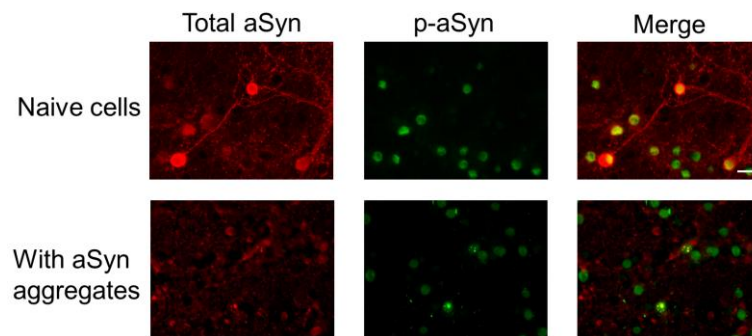
SI Fig. S5

Levels of synaptic proteins upon exposure to aSyn aggregates. Levels of pre-synaptic (synapsin, synaptophysin) and post-synaptic (PSD95) proteins are quantified by immunoblot analysis in cultures exposed to aSyn species. MW, molecular weight/molecular mass. *, $p < 0.05$; **, $p < 0.01$ for comparison between samples and their appropriate vehicle control.
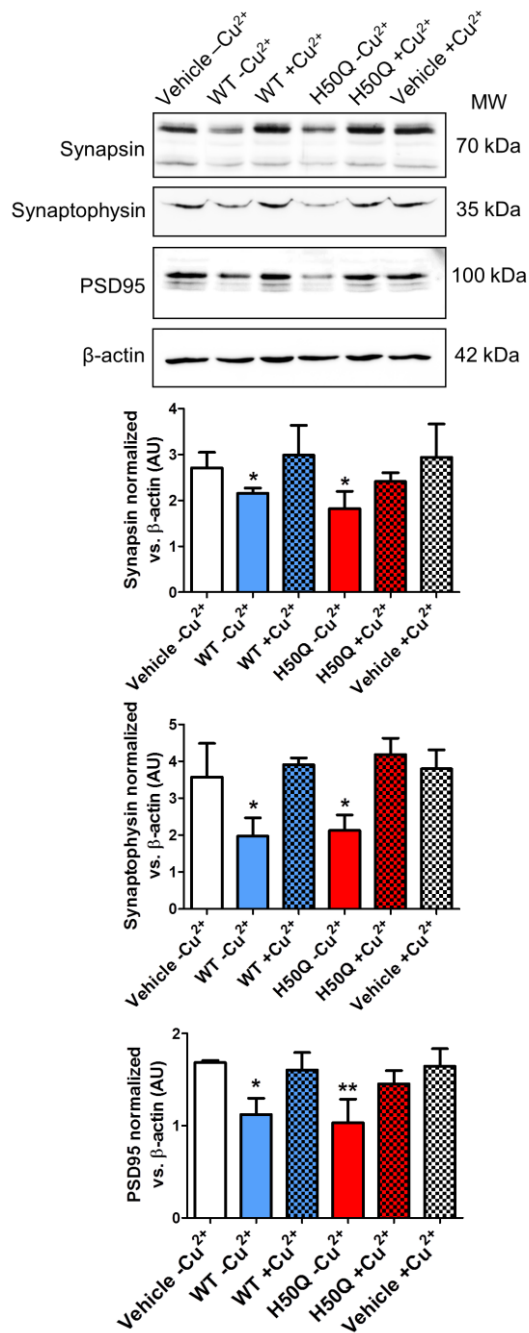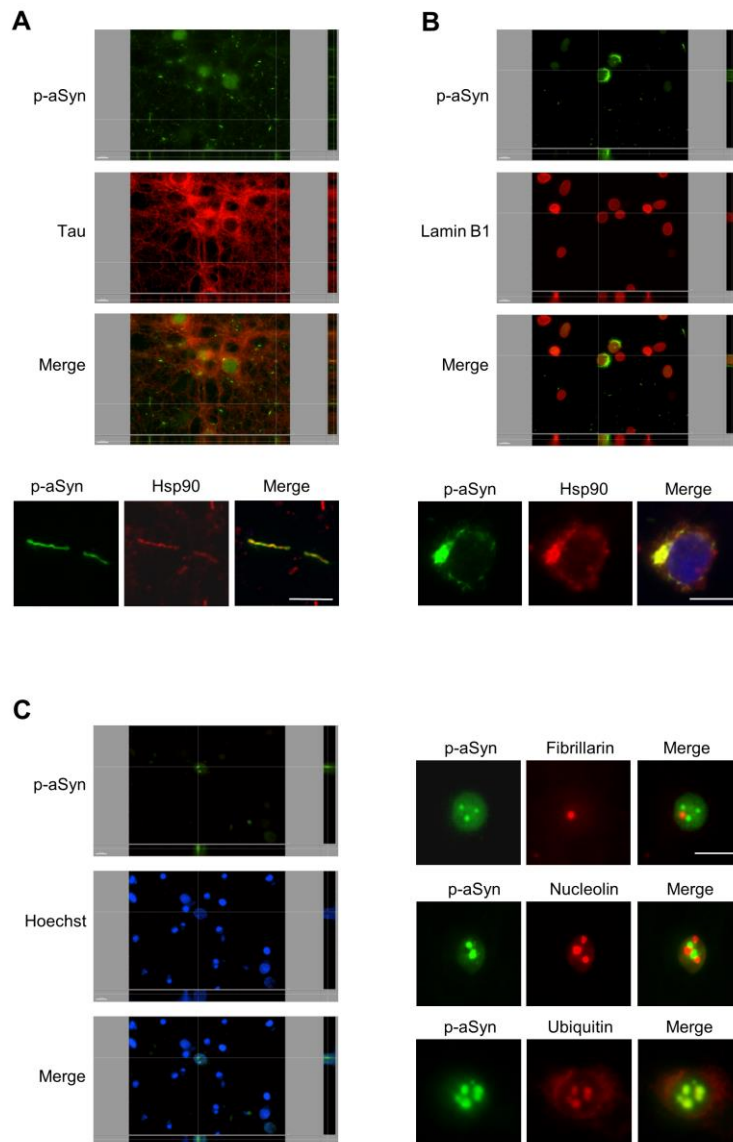
SI Fig. S6

Colocalization between total aSyn and p-aSyn. Double immunostaining was performed with Syn-1 antibody, which stains for total aSyn, and p-aSyn (S129) antibody in untreated or vehicle controls (*Top*) and treated (*Bottom*) cells with aSyn aggregates. (Scale bar, 20 µm.)

 Characterization of the S129 p-aSyn inclusions. A. Partial co-localization of neuritic inclusions in Tau-positive projections (*Top*) and with Hsp90 (*Bottom*). **B.** Perinuclear morphology of perykarial inclusions determined with Lamin B1 co-staining (*Top*) and co-localization with Hsp90 (*Bottom*). **C.** Intranuclear location of nuclear inclusions determined with Hoechst co-staining (*Left*), exclusion from nucleolar structures determined with fibrillarin and nucleolin co-staining (*Right top and middle, respectively*) and co-localization with ubiquitin (*Right bottom*). (Scale bars, 10 μm.)

SI Fig. S8

Levels of stress-associated proteins upon exposure to aSyn aggregates. A. Levels of heat shock proteins Hsp40 and Hsp70 are assessed by WB in cultures exposed to aSyn species. Treatments with pro-apoptotic drugs Staurosporin, MG132 and Thapsigargin are included as positive controls for inhibition of protein kinases, inhibition of proteasome and alteration of calcium homeostasis, respectively. **B.** Similarly to A, levels of CHOP are assessed. A longer treatment in positive controls was required in this case, as indicated. MW, molecular weight/molecular mass
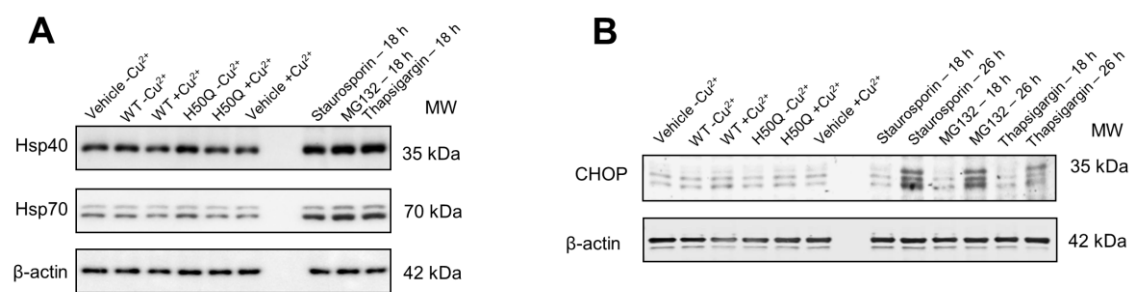
SI Materials and Methods

Purification of aSyn

aSyn WT and H50Q mutants were cloned in pET21 vector between the NdeI and XhoI restriction sites. Protein production and purification was performed in *Escherichia coli* BL21 cells as previously described (1, 2). Briefly, protein expression was induced with isopropyl beta-D-1-thiogalactopyranoside for 3 h at 37°C. Cells were recovered, boiled, and cell debris was discarded by centrifugation, including subsequent precipitation with streptomycin sulphate and acetic acid. Ammonium sulphate at 50% (wt/vol) was used to obtain an aSyn-enriched precipitate. This fraction was washed and further precipitated with ethanol 100% (vol/vol). Further purification using an anion-exchange HiTrap Q HP column (GE Healthcare) was performed in high-pressure liquid chromatography equipment with a constant gradient of 0-1 M NaCl. The integrity and purity of both aSyn variants were confirmed by mass spectrometry.

Aggregation of aSyn

After filtering through 100 kDa Amicon centrifugal tube (Millipore) to remove large aggregates, aSyn was aggregated at 70 µM in sterile PBS at pH 7.5 with sodium azide at 0.02% (wt/vol) in low-binding micro-tubes. $CuCl_2$ at 70 µM was added to the appropriate reactions. Aggregation buffers with and without $CuCl_2$ were prepared likewise to be used as vehicle controls. The kinetics of aggregation was performed at 37ºC under constant agitation and followed by mixing aliquots of each sample at selected time points with a solution of Th-T at 30 µM. Three independent experiments were performed in parallel. Th-T fluorescence was measured by exciting the sample at 450 nm while collecting the emission from 400 to 600 nm on a Jasco FP 8200 spectrofluorometer. The intensity peak at 482 nm was used to compare the degree of amyloid species present in each sample. Sedimentation assays were performed at the end time points of the aggregation kinetics. An aliquot of each sample was centrifuged at 20000 xg for 1 h and the amount of protein present on the supernatant was measured by Nanodrop to determine the remaining soluble aSyn in each sample. A freshly prepared sample was measured as a control. The aggregation kinetics of WT and H50Q aSyn (70 µM) with different $CuCl_2$ concentrations (35 µM, 70 µM and 140 µM) was performed in a 96 well plate, using the buffer and temperature conditions above described. A 1/8" diameter teflon-ball (Polysciences Europe) was introduced in each well to ensure high experimental reproducibility (3). Th-T fluorescence measurements were taken every 5 min on a SpectraMax Paradigm Multi-Mode Microplate Reader (Molecular Devices). Aggregation in the presence of iron was conducted

likewise adding 70 µM of FeCl$_2$. For live cell imaging experiments, H50Q +Cu^{2+} aggregates were labelled with ATTO 590 NHS-ester (Atto-Tec GmbH) following the manufacturer's recommendations and using sedimentation cycles as previously described to remove unbound dye (4).

Fourier transform infrared spectroscopy

ATR-FTIR analysis of the aggregated samples was carried out using a Bruker Tensor 27 FTIR spectrometer (Bruker Optics) with a Golden Gate MKII ATR accessory. 5 µL of each sample were placed in the centre of the diamond and dried with N$_2$. Each spectrum consisted of 16 scan accumulations measured at a spectral resolution of 2 cm^{-1} in a wavelength range between 1700 and 1500 cm^{-1}. Infrared spectra were fitted through overlapping Gaussian curves, and the amplitude, mass centre, bandwidth at half of the maximum amplitude, and area for each Gaussian function were calculated employing a nonlinear peak-fitting program (PeakFit package, Systat Software).

PK digestion analysis

Proteolytic reactions were prepared in low-binding microtubes containing aSyn aggregates and freshly prepared PK at final concentrations of 8.4 µM and 2.5 µM, respectively. Digestions were performed at 37°C under mild agitation and, at the indicated time points, they were stopped by adding sample buffer and immediately placing them at 100°C. Samples were resolved on Tricine-based protein electrophoresis and protein bands were stained with Coomasie brilliant blue. Alternatively, protein fragments were transferred to a Western-Blot (WB) membrane and simultaneously developed with Syn-1 and C-20 antibodies using a fluorescence-based system (Li-Cor Biosciences).

Human cell cultures

Human neuroglioma H4 cells were maintained at 37°C and 5% CO2 environment, in Dulbecco's modified Eagle medium (PAN) supplemented with 10% foetal calf serum and 1% penicillin-streptomycin. Cells were seeded in different well-plate formats, one day prior to transfection, and kept up to 48 h after transfection. Transfections were performed with calcium phosphate. Shortly, 3 h prior to transfection, fresh cell medium was added to the cells. DNA was diluted in 1x HBS buffer with 25 mM 4-(2-hydroxyethyl)-1-piperazineethanesulfonic acid, 140 mM NaCl, 5 mM KCl, 0.75 mM Na2HPO4·2H20, 6mM Dextrose, pH 7.1. After mixing, 2.5 M CaCl2 was added dropwise and vigorously mixed. Followed 20 min of incubation, the mixture was added dropwise to the cells. In the next morning cells were fed with fresh medium. 24 hours after

transfection, CuCl2 was added to the cell media with a final concentration of 1µM. Cytotoxicity was measured using the release of lactate dehydrogenase (LDH) into the culture medium, using a commercial LDH Cytotoxicity Kit (Roche). Basic LDH release was measured in non-transfected cells, and the maximal LDH release was measured by cell lysis in 2% (vol/vol) Triton X-100. Absorbance was measured with the Infinite M2000 PRO (Tecan Ltd) plate reader at 490 nm. Experimental values were calculated in percentages of the maximal LDH release and normalized to WT as a control.

<u>Primary cell cultures</u>

Primary cortical cultures from E18 embryos of WT rats were prepared as described with slight modification (5). Cells were cultured in Neurobasal (Gibco) supplemented with 5 µg/mL transferrin, 1X penicillin-streptomycin (Pan-Biotech), 0.5 mM L-glutamine and 1X B27 (Gibco). Fresh medium was added every 3-4 days. Cells were treated with sonicated aSyn species (labelled species when appropriate) at day-in-vitro (DIV) 9 and recovered at DIV 21. Final concentration of aSyn aggregates in the cultures was 1 µM and equivalent volume of vehicle buffers were employed as negative controls. When appropriate, cells were treated for 18 h or 26 h with the pro-apoptotic drugs Staurosporine (1 µM), MG132 (1nM) and Thapsigargin (100 nM). Cytotoxicity in primary cultures was assessed using the ToxiLight kit according to the manufacturer's instructions. Cell survival and apoptotic nuclei quantification was performed in 96-well plates (50000 cells/well). Immunostaining imaging was performed in 48-well plates (110000 cells/well) or 24-well plates with coverslips (250000 cells/well). WBs were performed from 12-well plates (500000 cells/well). Live cell imaging was performed in 35 mm µ-dishes (Idibi) containing 200000 cells cultured in phenol red-free medium. When necessary, neurons were infected with a GFP-overexpressing lentivirus at DIV 5 and treated with aSyn H50Q +Cu^{2+} labelled aggregates at 1 µM at DIV 9. Culturing conditions were the same as specified above. Pictures were obtained at 37ºC in culture medium without phenol red with a spinning-disc confocal microscope (Nikon/PerkinElmer).

<u>Immunostaining studies</u>

Cells were washed 3-times with sterile PBS and fixed with 4% (wt/vol) paraformaldehyde for 30 min at room temperature (RT). When appropriate, fixation was performed in the presence of 1% (vol/vol) Triton X-100 to remove soluble structures (6). Fixed cells were permeabilised and then blocked for 2 h at RT with 3% (wt/vol) bovine serum albumin. Primary antibodies (1:3000 for GFAP, Hsp90, Lamin B1, MAP2 and Tau; 1:1000 for aSyn Syn-1, rat-specific D37A6 aSyn, S129 p-aSyn, fibrillarin, nucleolin and ubiquitin) were incubated overnight at 4°C. Alexa

Fluor conjugated secondary antibodies were used at 1:2000 and incubated 1 h at RT. Nuclei were counterstained with Hoechst. Imaging was performed in a Leica DMI 6000B or in an Olympus XI81 microscope. Images were processed and analysed with Olympus ScanR software and ImageJ.

<u>Immunoblotting analysis</u>

Cells were washed with PBS and lysed in the presence of 25 mM Tris-HCl pH 7.5, 150 mM NaCl, 1% (vol/vol) Triton X-100 and a tablet of proteases inhibitors for 30 min on ice. Lysates were clarified by centrifuging at 14000 xg and 4°C for 1 h. 30 μg of total protein were mixed with sample buffer, boiled and applied onto SDS-PAGE protein gels. For soluble/insoluble fractionation, cell lysates were centrifuged to separate the supernatant (soluble fraction) and the pellet, which was washed and resuspended in lysis buffer supplemented with 2% (wt/vol) SDS. After a brief sonication, the resuspended pellets were centrifuged to obtain the insoluble fractions. Soluble and insoluble fractions were applied onto SDS-PAGE gels in a similar manner as total lysates. After electrophoreses, gels were transferred into polyvinylidene difluoride membranes, which were subsequently blocked for 1 h at RT (TBS + 5% (wt/vol) Milk + 0.1% (vol/vol) Tween). Primary antibodies (1:5000 for Syn-1 aSyn, C-20 aSyn, GFAP, synapsin and synaptophysin; 1:2000 for rat-specific D37A6 aSyn, S129 p-aSyn, CCAAT-enhancer-binding protein homologous protein (CHOP), Hsp40, Hsp70, MAP2, PSD95 and Tau) were incubated overnight at 4°C. Horseradish peroxidase conjugated secondary antibodies were incubated for 1 h at RT and membranes were developed. Images were processed and bands quantified with ImageJ software. A minimum of 3 independent experiments were performed for each case and statistical analyses were carried out with GraphPad Prism following the recommended software settings for the present experiments (Anova with Tukey's post-test). $p < 0.05$, $p < 0.01$ and $p < 0.001$ were represented as *, ** and ***, respectively, when comparing each condition with its appropriate vehicle control. $p < 0.05$ and $p < 0.01$ were represented as # and ##, respectively, when comparing among different conditions. Error bars indicate standard deviation.

References of SI Materials and Methods

1.   Volles MJ, Lansbury PT (2007) Relationships between the Sequence of Alpha-Synuclein and its Membrane Affinity, Fibrillization Propensity, and Yeast Toxicity. *J Mol Biol* 366(5):1510–1522.

2.   Chutna O, et al. (2014) The small GTPase Rab11 co-localizes with α-synuclein in intracellular inclusions and modulates its aggregation, secretion and toxicity. *Hum Mol Genet*

23(25):6732–6745.

3.   Giehm L, Lorenzen N, Otzen DE (2011) Assays for α-synuclein aggregation. *Methods* 53(3):295–305.

4.   Hansen C, et al. (2011) α-Synuclein propagates from mouse brain to grafted dopaminergic neurons and seeds aggregation in cultured human cells. *J Clin Invest* 121(2):715–725.

5.   Tönges L, et al. (2014) Alpha-synuclein mutations impair axonal regeneration in models of Parkinson's disease. *Front Aging Neurosci* 6:239.

6.   Volpicelli-Daley LA, et al. (2011) Exogenous alpha-Synuclein Fibrils Induce Lewy Body Pathology Leading to Synaptic Dysfunction and Neuron Death. *Neuron* 72:57–71.